



A Review of Image Denoising Techniques

Hibaa Ali Rashid Al-Ibraheemi¹, Ali Abdulazeez Mohammedbaqer Qazzaz²,

¹Faculty of Education ,University of Kufa, Computer Science Department, Iraq, hibaa.alibraheemi@student.uokufa.edu.iq
²Faculty of Education University of Kufa, Computer Science Department, Iraq, alia.qazzaz@uokufa.edu.iq
*Corresponding author E-mail: hibaa.alibraheemi@student.uokufa.edu.iq

https://doi.org/10.46649/fjiece.v4.2.2a.20.9.2025

Abstract. Noise is undesired information in an image that appears during image capturing, transmission, coding, and processing steps, negatively impacting visual quality and obscuring important details. Image denoising is therefore a central problem in both image processing and computer vision, aiming to suppress such distortions while preserving essential structural information. Our paper aims to shed light on recent research in image denoising techniques, evaluate the performance of prominent methods, highlight research gaps, and identify areas for further study.

Keywords: Noise; Gaussian noise; Salt and Pepper; CNNs; GANs.

1. INTRODUCTION

Digital image plays a vital role in various applications. Due to various influences, including transmission channels and environmental factors, images are inevitably corrupted by noise during capture, compression, or transmission, resulting in degradation and loss of informative image details. The essential image processing tasks are negatively impacted by noise. Image denoising is necessary to recover a clean image from a noisy one without compromising image details. Image denoising is a technique used to overcome image problems, such as signal distortion and unwanted noise, for authentic image restoration. In fact, image denoising is an increasingly important issue and still an open task; researchers have proposed numerous approaches to effectively remove noise while preserving image information. It is widely acknowledged that image sharpness details and noise are high-frequency components, which are difficult to recognize in the image denoising process; therefore, some details are inevitably lost during the denoising process.

2. TYPES OF NOISE IN IMAGES

Many types of noise can adversely affect the images. These noises can arise from various sources. In general, noise can be categorized into additive noise sources, which are associated with image capturing devices, invalid memory addresses, or shortcomings of image capturing devices, such as cameras, misaligned lenses, poor focal length, scattering, multiplicative noise, and impulse noise. The impulse noise, in turn, is classified into dynamic (random) and static noise, which tend to modify pixel values randomly [1]. Noise removal from the image is a complicated process without Initial knowledge of a noise model. Therefore, pre-defining noise models is essential in applying the image denoising techniques





2.1. GAUSSIAN NOISE:

This type of noise follows a Gaussian distribution. The primary source of Gaussian noise manifests during acquisition of the image, such as Sensor Noise Presented by low illumination or high temperature values, and electronic circuit noise. It is generally either additive or multiplicative, and it concerns only zero-mean additive noise. The key aspect of a Gaussian distribution is calculating the mean of a random variable for a stationary Gaussian; there is no better than a linear average. This is why Gaussian noise is the worst scenario for nonlinear filters in image restoration, as the linear filter's enhancement is least effective for Gaussian noise. At each point, Gaussian noise is independent of pixel value intensity [2]. Equation (1) and Figure (1) illustrate the PDF of Gaussian noise. It is likewise known as random variation, impulsive noise, or enhancer noise (6).

$$F(g) = \frac{1}{\sqrt{2\pi\sigma^2}} \frac{-(g-\mu)^2}{2\sigma^2}$$
 (1)

Where F(g)= Gaussian distribution noise in the noisy image, σ is the standard deviation, and μ is the mean value.

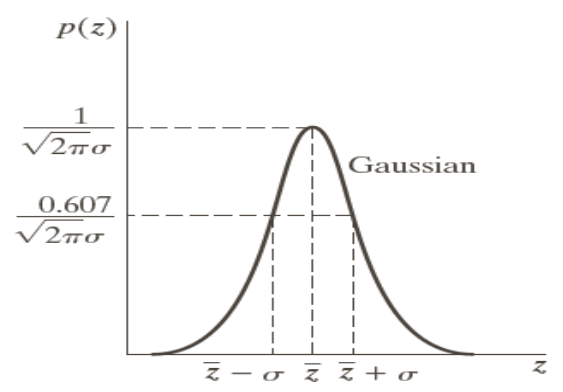


Fig. 1. PDF of Gaussian Noise.

2.2. SALT AND PEPPER NOISE (IMPULSE NOISE)

This model of noise appears when the image signal rapidly and suddenly changes, and may be caused by malfunctions and shortcomings of the imaging device, timing errors during the digitization process, etc. Salt and Pepper noise represented by black and white pixels. Salt and pepper noise, also known as data drop noise, occurs when there is a change in pixel values. However, salt and pepper noise partially corrupted the image by either increasing or decreasing the minimum or maximum pixel value [2]. This noise can have a minimum (0) or a maximum (255) value. For salt noise, the values are close to 255, and for pepper noise, they are close to 0. The intensity values typically fall at either the minimum or maximum levels.[3]

$$\eta(x,y) = \begin{cases} 0, & Pepper \ noise \\ 255, & Salt \ noise \end{cases}$$
(2)





The PDF of Salt and Pepper noise is represented by:

$$p(z) = \begin{cases} pa & For \ z = a \\ pb & For \ z = b \\ 0 & others \end{cases}$$
 (3)

Where P (z) represents the Probability density function, and z is the random variable that represents noise.

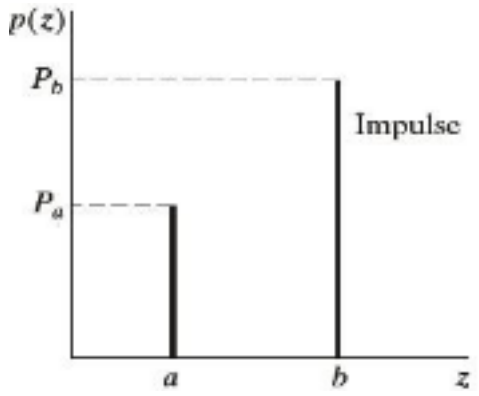


Fig. 2. PDF of Salt and Pepper Noise.

2.3. SPECKLE NOISE

Speckle noise is multiplicative in nature. This type of noise arises in imaging systems that involve laser systems, Synthetic Aperture Radar (SAR) imagery, and ultrasound images. The source of this noise is attributed to random interference between the coherent returns. The source of this noise is the random overlap of coherent returns. Speckle noise follows a gamma distribution as illustrated in Figure 3. Its probability density function is subjected to a gamma distribution.[4]

$$F(g) = \frac{g^{a-1}}{(a-1)!a^a} e^{\frac{-g}{a}}$$
 (4)

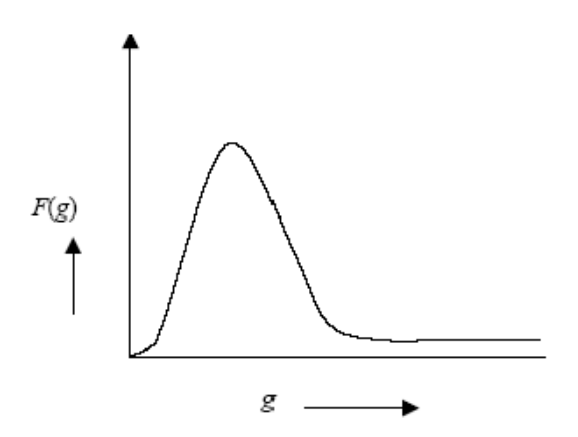


Fig. 3. PDF of Speckle Noise.





2.4. POISSON NOISE (PHOTON NOISE)

This model of noise appears due to the statistical nature of electromagnetic waves like visible light, X-rays, and gamma rays. In gamma-ray imaging systems and medical X-ray imaging, these rays are emitted from their source and injected into the patient's body. The ray's sources are having random photon variations. The result gathered image demonstrates spatial and temporal fluctuations. Poisson noise is also called shot noise or quantum noise. This noise undergoes the Poisson distribution [5], which is given as:

$$p(f_{(pi)} = k) = \frac{\lambda^{k} i^{e^{-\lambda}}}{k!}$$
Where λ is the mean and $k = 0, 1, 2, ...$

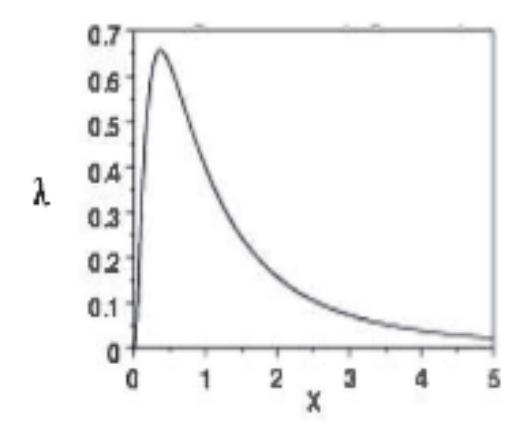


Fig. 4. PDF of Poisson Noise.

2.5. STRUCTURED NOISE

Structured noise is periodic and aperiodic in nature. The electronic components' interferences cause such noise; communication channel noise exists in two forms: structured noise and unstructured noise. Structured noise is also referred to as low-rank noise. It is more beneficial to leverage a noise model defined in a lower-dimensional space for signal processing. In a physical system, this noise model is transformed into a full score measurement space. In measurement space, we can be sure that the resulting low-rank noise displays a physical system-based structure. The structured noise model is expressed in Equations (6) and (7), respectively [5].

$$y_{(n)} = x_{(n,m)} + v_{(n)}$$

$$y_{(n)} = H_{(n,m)} * \theta_{(m)} + s_{(n,t)} * \emptyset_{(n)} + v_{(n)}$$
(6)

Where y represent the received image, n = rows, m = columns, H represent Transfer function of linear system, S indicates the Subspace, t is the rank in subspace, φ signifies the underlying process which exciting the linear system (S), θ indicates the signal parameter excites or sets initial conditions, linear system H is used to generate original signal x relative to n vector random noise (v(n))[6]. The figure displays the image after applying the Structured noise.





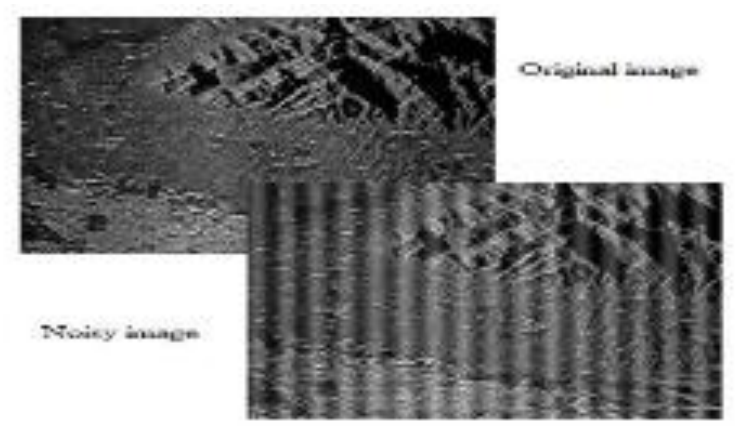


Fig. 5. Structured Noise.

2.6. QUANTIZATION NOISE

It's also called Uniform noise. Where the detected image pixels are mapped into discrete levels, the distribution is characterized by uniformity, as illustrated in Figure 6.

$$p(z) = \begin{cases} \frac{1}{b-a} & \text{if } a \leq z \leq b \\ 0 & \text{otherwise} \end{cases}$$
 (8)

Where the \bar{z} Represent the mean of the density function, given by $\bar{z} = \frac{(a+b)}{2}$ and its variance presented by $\bar{z} = \frac{(a+b)}{2}$.

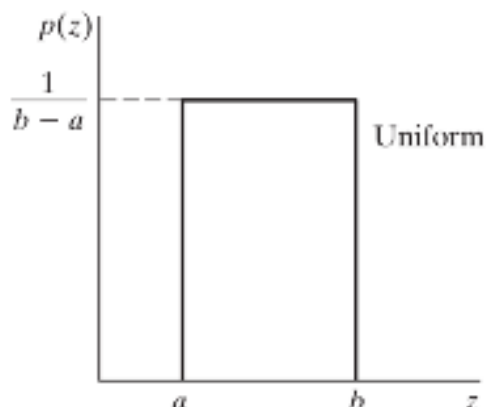


Fig. 6. PDF of Quantization Noise.

2.7. BROWN NOISE (FRACTAL NOISE)

It's known as Brownian noise; in a sound signal, it changes momentarily in a random manner. Brown noise is an integration of multiple types of noise involving white noise, blue noise, and pink noise. Brown noise energy is concentrated in the low frequencies. it's somewhat similar to red light, having a low frequency[7]. Statistically, fractional Brownian noise is referred to as fractal noise. The fractal noise is caused by natural processes. It is different from the Gaussian process. In mathematical terms, the motion of fractional Brownian motion can be represented as a zero-mean Gaussian process (BH) as demonstrated by Equations (9) and (10), respectively. [2]





$$B_{H}(0) = 0$$
 (9)
 $E\{|B_{H(t)} - B_{H(t-\Delta)}|^{2}\} = \sigma^{2} |\Delta|^{2H}$ (10)

2.8. PERIODIC NOISE

This model of noise is caused by electronic interference. A spatial dependency and sinusoidal pattern are specific characteristics of periodic noise, which display in the frequency domain as conjugate spots. It can be denoised by applying a notch filter or narrow-band reject filter [5].



Fig. 7. Periodic Noise.

2.9. GAMMA NOISE

In general, Gamma Noise appears in the laser-based images. Gamma Noise is also called Erlang noise. It follows the Gamma distribution [8].

$$f(x) = \begin{cases} \frac{a^{x}z^{b-1}}{(b-1)!} e^{-az} & for \ z < 0\\ 0 & for \ z \ge 0 \end{cases}$$
 (11)

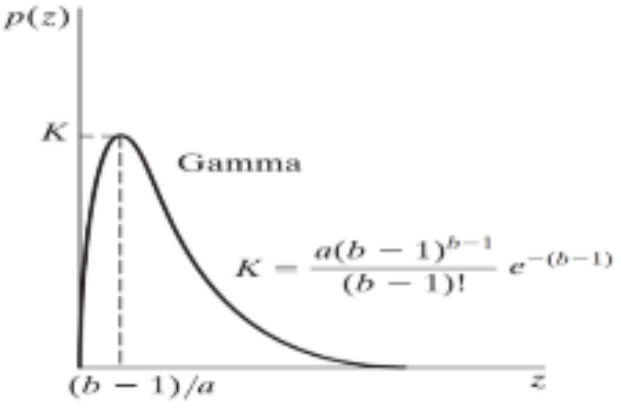


Fig. 8. PDF of Gamma Noise.





2.10. RAYLEIGH NOISE

Rayleigh noise is present in radar range images; the PDF is given as [5].

$$p(z) = \begin{cases} \frac{2}{b} (z - a)e^{\frac{-(z - a)^2}{b}} & \text{for } z \ge a\\ 0 & \text{for } z < a \end{cases}$$
 (12)

Where variance $\sigma^2 = \frac{b(4-\pi)}{4}$ and mean $\mu = a + \sqrt{\frac{\pi b}{4}}$

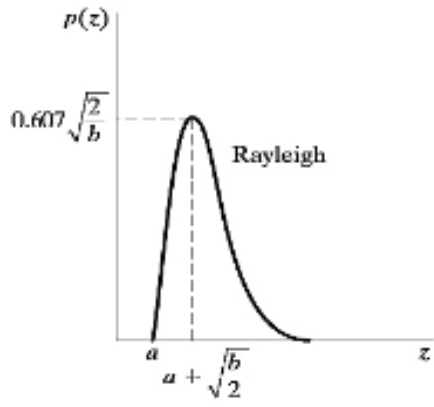
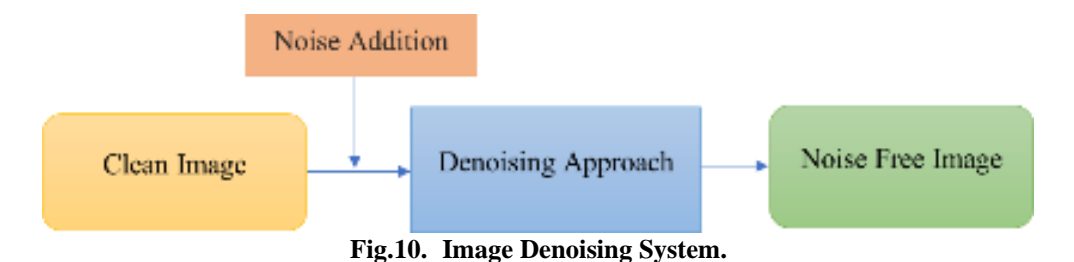


Fig. 9. PDF of Rayleigh Noise.

3. IMAGE DENOISING TECHNIQUES

A considerable amount of literature has been published on image Denoising utilizing various techniques, ranging from traditional approaches such as Wiener filters and median filters, to advanced approaches like Block-Matching 3D Filtering (BM3D), and wavelet-based thresholding. In the present era, deep learning techniques, which involve Generative Adversarial Networks (GANs) and Convolutional Neural Networks (CNNs), have exhibited remarkable success in addressing complex patterns of noise and achieving high-quality results across diverse noise levels. The image denoising system is illustrated in Figure 10.







3.1. IMAGE DE-NOISING-BASED FILTERING

Filtering is a method in image processing used for various tasks, such as noise reduction, resampling, interpolation, and edge detection. In denoising tasks, the filtering methods focus on assessing and detecting noisy pixels quickly and removing them. The filter selection is based on the amount and type of noise that exists in an image. The filters can be classified into three classes: linear filters, nonlinear filters, and adaptive filters.[9]

3.1.1. LINEAR FILTER

It is homogeneously applied to the entire image. Sometimes this blurs image detail, such as sharp edges and lines. A linear filter alone is not commonly adopted to remove noise due to the blurring. It often comes as a base step for other noise reduction methods. The linear filter operates based on identified conditions, such as linearity and shift invariance [13].

Mean filter: Mean filtering smooths an image by decreasing the intensity gradient between the pixel and the next one. The arithmetic mean filter can be represented by the following equation [10]. It is the simplest spatial filter, relying on the moving window principle, which replaces the centre value of the sliding window with the average pixel value in the kernel [9].



Clean Image: Lena



Gaussian Noise



Mean Filter 3x3

Fig.11. Image Denoising using Mean Filter.

Wiener filter: It is considered the most essential methodology for noise reduction, and it can be defined in the time domain or the frequency domain. The time domain Weiner filter has been obtained by minimizing the value of MSE between the given image and its assessment [10]. Wiener filtering can easily blur sharp edges. Weiner filtering equation for noise image adaptive retrieval is expressed as:

$$f(x,y) = m(x,y) + \frac{\sigma^2(x,y)}{\sigma^2(x,y) + \sigma^2(x,y)}$$
 (13)











Clean Image: Lena

Gaussian Noise

Wiener Filter 3x3

Fig. 12. Image Denoising using Wiener Filter.

3.1.2. NON-LINEAR FILTER

Non-linear filters are suitable for denoising salt and pepper noise from the image, especially in low-intensity level scenarios. The non-linear filters, such as the median filter, which is a simple order-statistics filter, are less sensitive to outliers than the mean filter and can remove these outliers while retaining sharp details of the image. The median filter is used to eliminate the intensity variation between pixels in the image [13].

• Median filter: It is an order statistic filter; it is also based on the sliding window principle, and it processes a given image pixel by pixel. Each pixel's value is substituted with the median value of a set of neighbouring pixel values. it is the most commonly used non-linear filter, but in high noise level scenarios, it may not remove the salt and pepper noise effectively from the images [3]. The Median filter exhibits excellent capabilities of noise reduction; it is especially effective in the presence of salt and pepper noise, with less blurring compared to linear smoothing filters with a similar size [11].

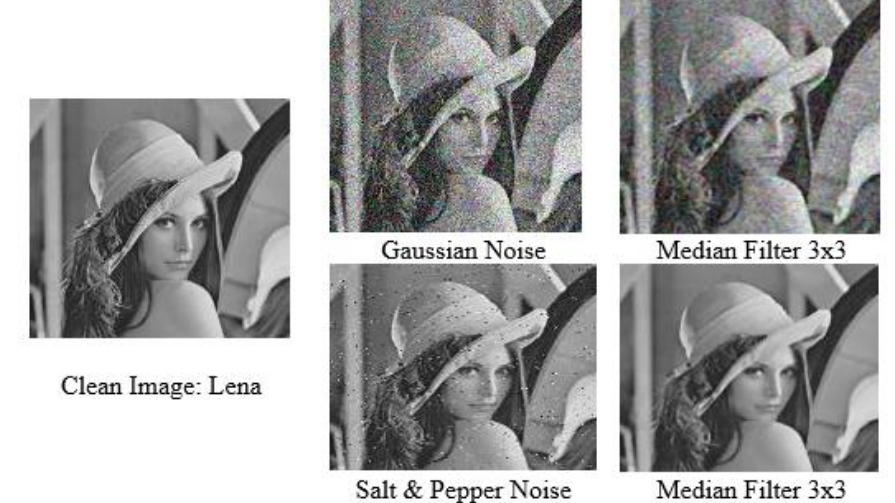


Fig. 13. Image Denoising using Median Filter.

 Gaussian filter: The Gaussian filter is a nonlinear, non-uniform low-pass filter. It is utilized for removing noise and detail from the image while adding blur effects to the resulting image. In a Gaussian filter, the weights are set for the smoothing purpose based on the outline of the Gaussian function [10]. The Gaussian filter has a bell-shaped curve; the standard deviation controls the level





of blur and tightness of the bell shape [12]. It does not effectively remove salt & pepper noise [9]. The equation of the Gaussian filter is expressed as:

$$G(x,y) = \frac{1}{2\pi\sigma^2} e^{-\frac{x^2 + y^2}{2\pi\sigma^2}}$$
 (14)









Clean Image: Lena

Gaussian Noise

Gaussian Filter 3x3

Gaussian Filter 5x5

Fig. 14. Image Denoising using Gaussian Filter.

3.1.3. ADAPTIVE FILTERS

These filters can selectively tailor their behaviour depending on local image variance by dynamically increasing the window size, weight, and threshold value. It performs less smoothing in larger image variances to preserve informative content in the image; if the image variance is slight, it performs high smoothing. So, it achieves better results compared to linear filtering [13].

Hybrid adaptive filters, which combine linear and nonlinear mechanisms, integrate iterative adjustments of thresholds and parameters according to noise density, providing a robust solution for handling diverse noise scenarios while striking a balance between denoising efficiency and detail preservation. Numerous studies, such as [14] and [15], have proven that this approach achieves better results compared to single-method filtering.

3.2. IMAGE DENOISING BASED DEEP LEARNING

Deep learning (DL) is a branch of machine learning that has led to significant innovations in artificial intelligence. A key aspect of DL is that it permits progress in learning through successive layers of progressively impactful representations.

3.2.1. NEURAL NETWORK

Neural network is a mechanism assigned to predictions in DL. It works by following a simple mental model; the information appears in a distilled format suitable for handling a particular problem after passing through the input layer and successive layers. A neural network is a highly flexible model that can achieve high prediction accuracy and solve a wide range of issues. The neuron is a building block of each layer. In the input layer, the neuron represents a feature. At the neuron core, an affine transformation is applied to its input, which is subsequently routed to an activation function. The affine transformation represents the dot product between a trainable weight and a matrix of feature vectors, followed by an offset term. The trainable weights matrix is adjusted during training to minimize a loss function that serves as a measure of the model's





predictive accuracy. Commonly used loss functions include the mean square error (MSE) for regression and the cross-entropy for classification problems. Neural networks have numerous hyperparameters, including the learning rate, activation function, batch size, and the choice of optimizer. The backpropagation algorithm plays an essential role in the NN work, as it efficiently calculates the loss function for all parameters in the training [16]. In the 1980s, Fukushima was the first to apply neural networks to image processing, and he proposed a self-organized network that learns without a teacher. For image denoising, Yi-Wu Chiang and Barry J. Sullivan presented an improvement to a neural network technique for single-image restoration, introduced by Zhou et al. After that, weighting factors were applied in the neural network for the removal of complex noise. A feedforward network was proposed to reduce computational complexity, thereby striking a balance between performance and denoising efficiency. It can smooth the given degraded image using Kuwahara filters, and the mean squared error (MSE) is used as the loss function. the mean squared error (MSE) was used as a loss function.

- Traditional neural networks (NNs) faced major limitations. They demanded high computational costs for large images and suffered from a trade-off between denoising efficiency and performance [Tamura, 1989]. They also required tedious manual parameter tuning, usually handled only one denoising task, and lacked flexibility and scalability for real-world use [Fukushima, 1980; Lucas, Iliadis, Molina, & Katsaggelos, 2018]. These problems underscore the urgent need for more effective and generalized techniques in image denoising[17].
- CNN for image denoising: CNNs are supervised deep learning techniques; in this technique, the learning process is based on labelled data. The CNNs generally benefit significantly from the availability of large training datasets to achieve a good performance [18]. CNN is defined by its local receptive field structure, which enables it to perceive better images, much like the human eye. It efficiently extracts and learns the features of images, with fewer parameters compared to other MLPs, and achieves better performance than MLP-based algorithms. After several improvements on CNNs, such as batch normalization and skip connections, many problems can be effectively alleviated. [19]. In mathematical terms, the CNN is constructed from three types of layers: the first two layers, convolution and pooling, which are responsible for feature extraction, while a fully connected layer is the third, which routes the extracted features into the output to make a decision. The figure (15) illustrates a simple CNN denoising model involving three convolutional layers. The convolution layer is composed of a set of mathematical linear operations, playing a vital role in CNN [20]. CNNs are characterized by efficient inference utilizing the GPU's parallel processing capabilities, which demonstrates a powerful capacity in terms of prior modeling. On the other hand, many of the deeper CNNs are very difficult to train for denoising tasks and suffer from a saturation of performance [21].

CNNs with a deep configuration can adapt to learning, so they are considered the most favoured approach for image denoising. Following the remarkable results of the ImageNet Large Scale Visual Recognition Competition (ILSVRC) in 2012, CNNs have garnered increasing interest and become a crucial method in the computer vision domain, achieving expert-level performance in various fields [20].





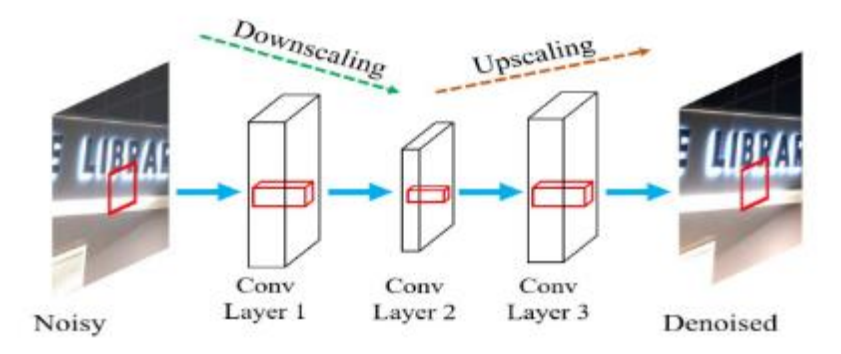


Fig. 15. A simple CNN denoising model.

• GANs-based image denoising: A generative adversarial network (GAN) is a novel and powerful class of deep generative models. GANs overcome the issues associated with Markov Chain Monte Carlo (MCMC) training, which used backpropagation for training. They can learn sophisticated and multi-dimensional patterns implicitly across various data types. GAN was proposed by Goodfellow in 2014. The key idea of GANs is based on the concept of a two-player zero-sum game. Within GANs, adversarial learning is employed to train both the generator and the discriminator, as illustrated in the figure. GANs aim to generate new data samples from the estimated distribution of real data samples. It demonstrates the ability to handle complex distributions and produce impressive results [22].

GANs have been successfully applied to several domains and tasks, effectively addressing the issues of limited and imbalanced data in practical engineering applications. The GCBD paper introduced GAN to image denoising for the first time. In this paper, the authors create paired-image data by training a generative network to produce noise, which is then used to train a denoising network, such as DnCNN [23]. After that, the researchers create a number of GAN variants, with innovations involving improvements to the model structure, novel applications, theoretical extensions, and more. Tripathi et al [24] apply GAN to recover clean images by leveraging Latent Vector Recovery (LVR) with the Sharpness Attribute to find the nearest point on the GAN manifold. ZhiPing et al. [23] proposed a GAN with a new generator network trained using a new loss function to calculate the divergence between the distributions of clean and denoised images. Chen et al [25] introduced a GAN-based approach with a Detail Loss to maintain informative details in texture-rich regions and achieve more visually realistic results during the denoising task.

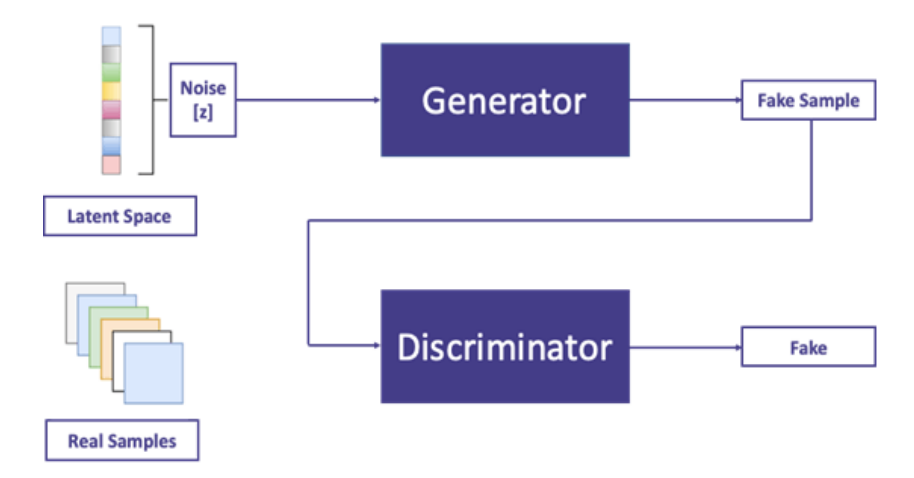


Fig. 16. The basic structure of the GAN model.





GANs suffer from an issue; they cannot generate diverse samples. Although they are trained on data from multiple models, this limitation is known as the mode collapse problem. The non-convergence and instability challenges arise during training, causing the generator to stop receiving necessary gradient updates to enhance its outputs, and training stagnates because the generator loses the ability to learn and create realistic samples. Several recent advances have focused on addressing the issue associated with GANs mentioned above [26].

4. DENOISING SYSTEMS:

To date, many studies have been published and introduced to denoise the Gaussian noise from various image types. Numerous studies utilizing CNNs for this purpose, such as Wencong. Wu et al. [27], have developed an Image blind denoising network (DCANet) based on a Dual CNN with a Spatial and Channel Attention Module (SCAM), applied a Noise Estimation Network for noise level predictions and distribution in the image, allowing adaptive denoising. On the Set12 dataset with a noise level of 75, the DCANet achieves a PSNR of 25.75 and an SSIM of 0.7458.

Sarkar et al.[28] provided an attention-guided CNN (ADNet) model. They have implemented median filters on all image feature channels and increased the dilation convolution ratio to expand the corresponding field size, which resulted in image denoising. After quantitative analysis of the BSD500 dataset, the ADNet model achieves a PSNR of approximately 26.05.

Singh et al. [29] applied DNN to address Gaussian noise, presenting a Residual Deep Neural Networks framework (ResDNN) and rectified linear unit (ReLU) activation, for denoising natural images. ResDNN framework achieves an overall PSNR of 31.397 dB in the result on the Set12 dataset. The ResDNN represents a significant advancement in the pursuit of high-quality image restoration. The framework commonly involves resizing images for training a denoiser, which can lead to information loss.

Zheng et al. [30] leverage a cloud-based image denoising approach that involves deep neural networks DNNs integrated with cryptographic techniques such as secret sharing and garbled circuits to preserve privacy. The proposed approach jointly addresses the data without revealing the real content. With σ equal to 15, the approach achieved PSNR values of 36.18 for Plaintext and 35.94 for Secure. The security approach can be extended to support more complex types of DNN, such as deep convolutional neural networks.

P. Liu et al. [31] proposed the Deep Regulated Convolutional Network (RC-Net), which utilizes regulated subnetwork blocks with skip connections for image restoration. The results clearly demonstrated that RC-Net consistently exhibits high efficacy, with an average PSNR of 32.87 dB. The RC-Net combines large and small convolution filters to make a balance between the network's generalizability and performance. BSD200.

Meanwhile, Zhue et al. [32] proposed a GAN-based denoising network, which constructs a robust denoising network with triple subnetworks supported by an optimization algorithm (OA). Although the constructed network requires improvement in denoising effect at low noise levels to achieve optimal performance in various noise environments, it exhibits good practicality in many applications, such as target detection and recognition. The experimental results using the BDS500 dataset show that at a noise level of 100, the model achieved a PSNR of 24.71 and an SSIM of 0.7640.

Interestingly, many papers employing classical Gaussian image denoising techniques with specific improvements, as stated in [33], have proposed a Gaussian mixture model (GMM) by Wei et al. The model defines pixel similarity by calculating the L2 norm between the Gaussian mixture models of two pixels and combining it with their spatial distance, allowing for a detailed comparison between pixels. experimental results show that the suggested model can effectively remove noise while preserving image detail information. The GMM model achieves 16.969 in terms of PSNR, testing on the Academy image from the Set12 dataset with noise intensity equal to 0.2.





Ye et al. [34] developed a novel Deep Cascade Broad Learning System (DCBLS). The DCBLS System combines cascaded feature mapping nodes and enhancement nodes for improved feature extraction and image denoising performance. The BSD400 dataset was used to test the system's performance with σ = 15; the system achieved an MPSNR of 32.2768 and a MISSM of 0.9396. The suggested system may not be suitable for denoising blind image scenarios, where noise features are unpredictable and a paired training dataset is unavailable.

Golshan et al. [35] introduced a novel Fuzzy Hysteresis Smoothing (FHS) denoising method that expands the norm by combining the fuzzy norm with a logarithmic nature to enhance the FHS accuracy and introduce a noise-free image. With the Set12 dataset at noise level 5%, the PSNR falls between 24.91 and 39.68. The FLAHS scheme is comparatively independent of the noise distribution, allowing it to be employed for other noise types by adjusting specific parameters without incurring excessive overhead.

Averbuch et al. [36] introduced an image denoising scheme integrating a directional quasi-analytic wavelet packets (qWPs) based method with the Weighted Nuclear Norm Minimization (WNNM) denoising approach. The qWPdn scheme involves qWP transform, adaptive localized soft thresholding, and Image Reconstruction strategies. The averaged values of SSIM are 1.002 and 1.026, respectively. The qWPdn—WNNM scheme can efficiently restore texture details and edges even from substantially degraded images.

Yang et al. [37] proposed a framework that applies an ensemble learning technique to combine simple denoisers for more accurate modelling of noise-free image manifolds. The framework also incorporates established denoisers, such as BM3D, and focuses on the shrinkage denoising technique, making it effective when training data is limited. It attains an average PSNR of 28.10 at a noise density of 30%.

Dai et al. [18] propose a Learnable Global Spatio-Temporal Adaptive Network (LGSTANet) with an efficient architecture that comprises aggregation, alignment, and reconstruction. The LGSTA aggregation module was adopted for efficient restoration and enhancement. It utilized the BracketIRE dataset and achieved a PSNR of 29.82, representing an improvement of 0.91dB compared to other state-of-the-art methods.

Similarly, Pang et al.[38] developed the Recorrupted-to-Recorrupted R2R framework, which utilizes a DnCNN backbone and constructs statistically independent noisy pairs through recorruption. The framework produced competitive results; on BSD68 degraded with AWGN at $\sigma = 50$, it yielded 26.13 dB of PSNR and an SSIM of 0.709. On real-world SIDD datasets, it achieves 34.78 dB in PSNR terms, and SSIM of 0.898, coming very close to supervised models, thereby guaranteeing effectiveness where clean reference images are unavailable.

A Hybrid filtering-based denoising system for Salt and Pepper noise was developed by Gondal et al. [39] based on a global unsymmetrical trimmed median filter (GUTM) with the mathematical morphology (MM) technique. By using the Digital Mammogram Images Dataset, the GUTM–MM system achieved mean PSNR values of 52.31, 49.65, and 48.44 for Normal, Benign, and Malignant images, respectively. In terms of PSNR, this Hybrid system performs better than other techniques.

Li et al. [40] applied a probability statistics-based filtering method. Noise points are defined by setting a probability threshold based on their frequency in relation to effective image points. With the Set12 dataset, the PSNR remains higher than 41 dB for low-density noise, and the SSIM is stable above 0.9 under low-density noise conditions and above 0.75 under medium-density noise conditions. This method requires additional adaptation for high-density noise conditions, and predefined probability thresholds may need to be tuned for optimal results across all noise conditions.

Kumar et al.[41] proposed a novel quartile-based approach for reducing salt-and-pepper noise. The quartile values are calculated using a convolution window method, and noisy pixels are replaced selectively by categorizing the centre pixel based on quartile values. The approach achieves superior performance in extreme noise levels by using the MSRA dataset with a PSNR of 24.4248 at a 0.25 density level; meanwhile, it requires significant improvement in low-density noise scenarios (less than 20% noise).





Muna Majeed Laftah. [42] Conducted the Multiwavelet Transform (MWT) image denoising system. The proposed system processes the HH coefficient using the Tri-State Median filter (TSMF) and the Switching Median Filter (SMF), supported by various shrinkage rules, to remove noise while maintaining image details. The test images from set12 were corrupted with salt and pepper noise at varying levels of 5%, 10%, 20%, and 30% to evaluate the performance of the filters under different noise intensities.

Sikhakhane et al. [43] introduced two algorithms for Speckle noise removal from breast ultrasound database images: the hybrid filter, which is an aggregation of digital filters, and a five-layer Denoising Convolutional Neural Network (DnCNN) based algorithm. The hybrid filter performs better when the noise level ranges between 0.1 and 0.3, achieving a PSNR range between 29.99 and 25.85. When the noise level falls between 0.5 and 0.9, the DnCNNL5 achieves a PSNR range of 24.42 to 23.35, indicating better performance.

Shuo et al. [44] also proposed a Multi-Layer Fusion Enhancement Method based on Block Matching and 3D Filtering for Speckle Noise Denoising. The MLFE-BM3D scheme involves NSCT hard threshold denoising and enhancement, multiple image layers' combinations, and frequency domain enhancement techniques. For the Lena local image with noise variance $\sigma^2 = 1300$, MLFE-BM3D attains a PSNR of 28.9134. The long-time-consuming nature of the BM3D algorithm can be improved for robust denoising.

A model that targets the denoising of Gaussian, SAP, and Speckle noise in a non-drowsy faces image dataset was suggested by K. Hussein et al.[45] The model distinguished drowsiness features relies on a median filter to remove noise before classification. The reported results for salt-and-pepper noise, Gaussian noise, and speckle noise are 20.97, 20.43, and 19.78, respectively. The median filter may be less effective for specific types of noise, and its performance decreases under high noise densities, especially with speckle noise.

Satapathy et al. [46] used a frequency-based decomposition technique that utilizes bi-dimensional empirical mode decomposition (BEMD) to analyze the noisy image into intrinsic mode functions (IMFs) and a residue. Standard filters are employed to filter each component separately, removing noise from homogeneous areas in the MRI brain dataset images while maintaining structures such as edges and corners, and improving brightness.

In 2023, Uzakkyzy et al. [47] applied the Attentive GAN to process noisy images affected by Gaussian noise, SAP noise, and noise of lines and stripes from the Kaggle open-access database. Gaussian filtering-based processing was also applied to the clean image to enhance the final image quality further. With a noise level exceeding 50, the framework achieves a high SSIM value, lower Gloss and D-loss values, indicating improved performance.

Rafiee et al.[48] employ a selective convolutional (SeConv) block to prepare the network input for subsequent conventional layers and tackle the participating issue of pure noisy pixels in image reconstruction. This approach surpasses the existing innovative SAP denoising scheme by effectively preserving edges and image details. On the color BSD68 dataset, it achieves a mean PSNR of 34.73 dB and an SSIM of 0.947. The authors do not explicitly discuss SeConvNet issues, such as computational complexity or potential weaknesses in specific environments.

Many studies implement noise detection and classification models, such as [45], that involve classifying four noise types. Utilizing feature extraction via Wavelet Transform (WT), Dimensionality reduction, followed by a CNN to identify the type of noise for the classification task. By applying the PSA model to the Ancient mural image dataset, it achieves an accuracy of 99.25% for noise type classification. This model achieves highlighted performance in noise types classification compared with the model which introduced by Al Mudhafar et al [49] that is developed a model to determine the existence of noise in 9 classes noisy image dataset and then classifying the noise type based on deep SVM classifier combine with wavelet scatter for five noise types classification, including Gaussian, Salt & Pepper, lognormal, Speckle, and Rayleigh. The proposed model achieves an overall noise detection accuracy of 91.30%.





Table 1. The performance result of the denoising system.

Denoising Approach	Ref.	Dataset	Noise level	Performance index
Classical Methods	Zhue et al. [28],(2021)	BDS500	100	PSNR:24.71, SSIM:0.7640
	Golshan et al. [35], (2021)	Set12	5 - 50	PSNR:39.68- 24.91
	Gondal et al [39], (2021)	MIAS	30	PSNR: 52.31 , MSE: 0.37.
	Zhongshen Li. [40], (2022)	Set12	15	PSNR:40.0889, SSIM: 0.9210.
	Kumar et al. [41], (2021)	MSRA	0.25	PSNR: 24.4248.
	Muna M.Laftah, [42], (2021)	Set12	5-30	PSNR: 39.35.
	Averbuch et al. [36], (2023)	Set12	$\sigma = 100$	SSIM: 0.999/1.143
	Yang et al. [37], (2020)	Set12	$\sigma = 25$.	PSNR:28.93
CNNs	Ye et al. [34], (2021)	BSD400	$\sigma = 15$	PSNR: 32.2768, MISSM: 0.9396.
	Rafiee et al. [48], (2023),	BSD68	$\sigma = 15$	PSNR: 34.73, SSIM: 0.947
	Wencong Wu et al.[27], (2023)	set12	75	PSNR: 25.75SSIM: 0.7458
	Singh et al.[29], (2020)	Set12	$\sigma = 20$	PSNR: 31.397.
	Zheng et al.[30], (2021)	ChestX-ray8	15	PSNR: 36.18, 35.94
	Wu et al.[33], (2021)	Set12	0.2	PSNR: 25.75, SSIM: 0.7458
	P. Liu et al. [31], 2019	BSD200	70	PSNR:32.87, SSIM: 0.8961
	Sikhakhane et al.[43], (2024)	Breast ultrasound	0.5 - 0.9	PSNR: 24.42-23.35
	Shuo et al. [44],(2019).	set12	0.1 - 0.9	PSNR: 28.9134.
	L. M. Satapathy et al. [46], (2022)	MRI brain images.	0.01	PSNR: 27.53
	Dai et al. [18], (2021)	BracketIRE	NR	PSNR: 35.78, SSIM: 0.919
GAN	Zhue et al.[32], (2022)	BDS500.	100	PSNR: 24.71, SSIM: 0.7640
	Sarkar et al.[28], (2020)	BSD500	50	PSNR: 26.05
	Uzakkyzy et al. [47], (2023)	Kaggle open-access	50	SSIM is close to one

Across the cited studies, CNN-based denoisers typically achieve about 31-35 dB PSNR on Set12/BSD68 under AWGN, generally outperforming classical filtering at mid to high noise. while the GAN approach reports PSNR around 24-36 dB, it is affected by noise intensity, training data, and the inclusion of perceptual losses. In narrow or low-noise settings, Classical filtering can be competitive, but it degrades with higher σ and non-additive noise scenarios. In such a case, the comparability between the various approaches is limited because the studies differ in noise levels and characteristics, dataset domain, and image modality.

5. CONCLUSIONS

Numerous papers have investigated image denoising, and the field continues to expand; by contrast, denoising itself becomes challenging without an accurate understanding of the underlying noise models. Accordingly, this review synthesizes noise taxonomies and provides an extensive overview of prominent noise removal techniques in images.

In practice, the CNN-based denoising approach consistently outperforms classical filters, which remain competitive only in low-noise scenarios. Meanwhile, the GAN-based denoiser can deliver superior perceptual fidelity; however, it faces instability due to the adversarial training dynamics and its dependency on carefully tuned losses.

In summary, the field lacks a robust blind denoiser that efficiently handles multiple noise types, including multiplicative, additive, impulse, and structured noise, with spatial variation. Additionally, a Standardized system evaluation across diverse benchmark datasets, under noise intensities ranging from light to heavy levels, is necessary to assess its efficiency, ability to generalize, and capacity to handle various noise types. Future work should explore the strengths of CNNs and GANs through hybrid designs, trained with noise-conditioned, multi-objective perceptual losses, and a calibrated adversarial term to enable blind generalization.





REFERENCES

- [1] O. Joshua, J. S. Owotogbe, T. S. Ibiyemi, and B. A. Adu, "A Comprehensive Review On Various Types of Noise in Image Processing The Role of Robust ICT in Fostering Agricultural Extension, Rural Development and Food Security View project Image Processing View project A Comprehensive Review On Various Types of Nois," Artic. Int. J. Sci. Eng. Res., no. November, 2019, [Online]. Available: http://www.ijser.org
- P. P. Patro, "a Review on: Noise Model in Digital Image Processing," no. 2, pp. 14–19, 2016. [2]
- C. Saxena and D. Kourav, "Noises and Image Denoising Techniques: A Brief Survey," Certif. Journal; [3] Int. J. Emerg. Technol. Adv. Eng., vol. 9001, no. 3, pp. 878-885, 2008, [Online]. Available: www.ijetae.com
- Sahil Ali Akbar, "Analyzing Noise Models and Advanced Filtering Algorithm.". [4]
- [5] A. H. Lone and A. N. Siddiqui, "Noise models in digital image processing," Glob. Sci-Tech, vol. 10, no. 2, p. 63, 2018, doi: 10.5958/2455-7110.2018.00010.1.
- 吉原蓮人, 藤川晃希, 山重雄哉, and 松村遼, "Convolutional Neural Network による害獣検出," [6] vol. 6, pp. 5–6, 2017, doi: 10.12792/iiae2017.004.
- P. Kumer Rajvor, S. Jamaluddin Ahmad, S. Yasmin, and A. Hasan Dewan Rafi, "A review on: [7] Different type of noise model in digital image processing," Int. J. Eng. Appl. Sci., no. 2, pp. 14–19, 2022, [Online]. Available: www.ijeas.org
- A. Gupta, R. Mishra, and A. K. Singh, "Various Types of Noise and Filtering Techniques for Digital [8] Images: A Comprehensive Study," vol. 17, no. 10.
- I. Singh, "Performance Comparison of Various Image Denoising Filters under Spatial Performance [9] Comparison of Various Image Denoising Filters Under Spatial Domain," no. July, 2016, doi: 10.5120/16903-6969.
- [10] S. Bharati, T. Z. Khan, P. Podder, and N. Q. Hung, "A Comparative Analysis of Image Denoising Problem: Noise Models, Denoising Filters and Applications," Stud. Syst. Decis. Control, vol. 311, no. June, pp. 49–66, 2021, doi: 10.1007/978-3-030-55833-8_3.
- [11] N. N. Win, K. Khat, K. Kyaw, T. Z. Win, and P. P. Aung, "Image Noise Reduction Using Linear and Nonlinear Filtering Techniques," no. August 2019, 2021, doi: 10.29322/IJSRP.9.08.2019.p92113.
- [12] A. Mohammed, A. A. Selami, and A. F. Fadhil, "A Study of the Effects of Gaussian Noise on Image Features," no. April 2016, 2018, doi: 10.32894/kujss.2016.124648.
- [13] S. Guan et al., "Adaptive median filter salt and pepper noise suppression approach for common path coherent dispersion spectrometer," Sci. Rep., vol. 14, no. 1, pp. 1-18, 2024, doi: 10.1038/s41598-024-66649-y.
- [14] R. Radhika and R. Mahajan, "An adaptive optimum weighted mean filter and bilateral filter for noise removal in cardiac MRI images," Meas. Sensors, vol. 29, no. August, p. 100880, 2023, doi: 10.1016/j.measen.2023.100880.
- [15] D. Gautam, K. Khare, and B. P. Shrivastava, "A Novel Guided Box Filter Based on Hybrid Optimization for Medical Image Denoising," Appl. Sci., vol. 13, no. 12, 2023, doi: 10.3390/app13127032.
- [16] C. Palaiokostas, "Breeding evaluations in aquaculture using neural networks," Aquac. Reports, vol. 39, no. June, p. 102468, 2024, doi: 10.1016/j.agrep.2024.102468.
- [17] C. Tian, L. Fei, W. Zheng, Y. Xu, W. Zuo, and C. W. Lin, "Deep learning on image denoising: An overview," Neural Networks, vol. 131, pp. 251–275, 2020, doi: 10.1016/j.neunet.2020.07.025.





- [18] A. A. Rafiee and M. Farhang, "A deep convolutional neural network for salt-and-pepper noise removal using selective convolutional blocks[Formula presented]," Appl. Soft Comput., vol. 145, no. 0, pp. 1–18, 2023, doi: 10.1016/j.asoc.2023.110535.
- [19] C. Tian, Y. Xu, and W. Zuo, "Image denoising using deep CNN with batch renormalization," Neural Networks, vol. 121, pp. 461–473, 2020, doi: 10.1016/j.neunet.2019.08.022.
- [20] A. Patil and M. Rane, "Convolutional Neural Networks: An Overview and Its Applications in Pattern Recognition," Smart Innov. Syst. Technol., vol. 195, pp. 21–30, 2021, doi: 10.1007/978-981-15-7078-
- [21] L. Alzubaidi et al., Review of deep learning: concepts, CNN architectures, challenges, applications, future directions, vol. 8, no. 1. Springer International Publishing, 2021. doi: 10.1186/s40537-021-
- [22] K. Wang, C. Gou, Y. Duan, Y. Lin, X. Zheng, and F. Y. Wang, "Generative adversarial networks: Introduction and outlook," 2017. doi: 10.1109/JAS.2017.7510583.
- [23] L. D. Tran, S. M. Nguyen, and M. Arai, "GAN-Based Noise Model for Denoising Real Images," Lect. Notes Comput. Sci. (including Subser. Lect. Notes Artif. Intell. Lect. Notes Bioinformatics), vol. 12625 LNCS, pp. 560–572, 2021, doi: 10.1007/978-3-030-69538-5_34.
- [24] S. Tripathi, Z. C. Lipton, and T. Q. Nguyen, "Correction by Projection: Denoising Images with Generative Adversarial Networks," 2018, [Online]. Available: http://arxiv.org/abs/1803.04477
- [25] S. Chen, D. Shi, M. Sadiq, and M. Zhu, "Image denoising via generative adversarial networks with detail loss," ACM Int. Conf. Proceeding Ser., vol. Part F1483, pp. 261-265, 2019, doi: 10.1145/3322645.3322656.
- [26] M. M. Saad, R. O'Reilly, and M. H. Rehmani, A survey on training challenges in generative adversarial networks for biomedical image analysis, vol. 57, no. 2. Springer Netherlands, 2024. doi: 10.1007/s10462-023-10624-y.
- W. Wu, G. Lv, Y. Duan, P. Liang, and Y. Zhang, "DCANet: Dual Convolutional Neural Network with Attention for Image Blind Denoising arXiv: 2304.01498v2 [cs. CV] 17 Jun 2023," pp. 1–20,
- [28] R. Sarkar, "Gaussian Noise from Images," pp. 178–183, 2020.
- [29] G. Singh, A. Mittal, and N. Aggarwal, "ResDNN: Deep residual learning for natural image denoising," IET Image Process., vol. 14, no. 11, pp. 2425–2434, 2020, doi: 10.1049/iet-ipr.2019.0623.
- [30] Y. Zheng, H. Duan, X. Tang, C. Wang, and J. Zhou, "Denoising in the Dark: Privacy-Preserving Deep Neural Network-Based Image Denoising," IEEE Trans. Dependable Secur. Comput., vol. 18, no. 3, pp. 1261–1275, 2021, doi: 10.1109/TDSC.2019.2907081.
- [31] P. Liu, X. Zhou, Y. Li, E. B. M. D, and R. Fang, "Image Restoration Using Deep Regulated Convolutional Networks," 2019, [Online]. Available: http://arxiv.org/abs/1910.08853
- [32] M. L. Zhu, L. L. Zhao, and L. Xiao, "Image Denoising Based on GAN with Optimization Algorithm," Electron., vol. 11, no. 15, pp. 1–12, 2022, doi: 10.3390/electronics11152445.
- [33] H. Wei and W. Zheng, "Image Denoising Based on Improved Gaussian Mixture Model," Sci. Program., vol. 2021, 2021, doi: 10.1155/2021/7982645.
- [34] H. Ye, H. Li, and C. L. Philip Chen, "Adaptive Deep Cascade Broad Learning System and Its Application in Image Denoising," IEEE Trans. Cybern., vol. 51, no. 9, pp. 4450-4463, 2021, doi: 10.1109/TCYB.2020.2978500.
- [35] H. Golshan and R. P. R. Hasanzadeh, "Fuzzy Hysteresis Smoothing: A New Approach for Image Denoising," IEEE Trans. Fuzzy Syst., vol. 29, no. 3, pp. 686–697, 10.1109/TFUZZ.2019.2961336.
- [36] A. Averbuch, V. Zheludev, M. Salhov, and J. Hauser, "Cross-boosting of WNNM Image Denoising method by," pp. 1–30.





- [37] X. Yang, Y. Xu, Y. Quan, and H. Ji, "Image Denoising via Sequential Ensemble Learning," IEEE Trans. Image Process., vol. 29, pp. 5038–5049, 2020, doi: 10.1109/TIP.2020.2978645.
- [38] T. Pang, H. Zheng, Y. Quan, and H. Ji, "Recorrupted-to-Recorrupted: Unsupervised Deep Learning for Image Denoising," Proc. IEEE Comput. Soc. Conf. Comput. Vis. Pattern Recognit., pp. 2043–2052, 2021, doi: 10.1109/CVPR46437.2021.00208.
- [39] R. M. Gondal, S. A. Lashari, M. A. Saare, and S. A. Sari, "A hybrid de-noising method for mammogram images," Indones. J. Electr. Eng. Comput. Sci., vol. 21, no. 3, pp. 1435–1443, 2021, doi: 10.11591/ijeecs.v21.i3.pp1435-1443.
- [40] Z. Li, T. Luo, Y. Lv, T. Guo, and T. Lin, "A Digital Denoising Method Based on Data Frequency Statistical Filtering," Appl. Sci., vol. 12, no. 24, 2022, doi: 10.3390/app122412740.
- [41] K. Kumar, "A Quartile Based Novel Approach For The Reduction Of Salt And Pepper Noise 5 th International Conference on Next Generation Computing Technology (NGCT 2019) A Quartile Based Novel Approach for the Reduction of Salt and Pepper Noise," no. January 2020, 2021, doi: 10.2139/ssrn.3538583.
- [42] M. M. Laftah, "Image Denoising Using Multiwavelet Transform with Different Filters and Rules," Int. J. Interact. Mob. Technol., vol. 15, no. 15, pp. 140–151, 2021, doi: 10.3991/ijim.v15i15.24183.
- [43] K. Sikhakhane, S. Rimer, M. Gololo, K. Ouahada, and A. M. Abu-Mahfouz, "Evaluation of Speckle Noise Reduction Filters and Machine Learning Algorithms for Ultrasound Images," IEEE Access, vol. 12, no. June, pp. 81293–81312, 2024, doi: 10.1109/ACCESS.2024.3411709.
- [44] H. Shuo, Z. Ping, S. Hao, S. Yu, and W. Suiren, "Image Speckle Noise Denoising by a Multi-Layer Fusion Enhancement Method based on Block Matching and 3D Filtering Image Speckle Noise Denoising by a Multi-Layer Fusion Enhancement Method based on Block Matching and 3D Filtering," pp. 1–19.
- [45] M. K. Hussein, T. M. Salman, and A. H. Miry, "a Deep Learning Approach for Noisy Image Classification in Automated Driver Drowsiness Detection," J. Eng. Sustain. Dev., vol. 25, no. Special, pp. 1-73-1–80, 2021, doi: 10.31272/jeasd.conf.2.1.10.
- [46] L. M. Satapathy and P. Das, "A New Approach of Image Denoising Based on Adaptive Multi-Resolution Technique," Niger. J. Technol. Dev., vol. 19, no. 1, pp. 92–100, 2022, doi: 10.4314/njtd.v19i1.10.
- [47] N. Uzakkyzy et al., "Image noise reduction by deep learning methods," Int. J. Electr. Comput. Eng., vol. 13, no. 6, pp. 6855–6861, 2023, doi: 10.11591/ijece.v13i6.pp6855-6861.
- [48] S. Rahman, S. Pal, J. Yearwood, and C. Karmakar, "Robustness of Deep Learning models in electrocardiogram noise detection and classification," Comput. Methods Programs Biomed., vol. 253, no. May, p. 108249, 2024, doi: 10.1016/j.cmpb.2024.108249.
- [49] R. A. Al Mudhafar and N. K. El Abbadi, "Image Noise Detection and Classification Based on Combination of Deep Wavelet and Machine Learning," Al-Salam J. Eng. Technol., vol. 3, no. 1, pp. 23–36, 2023, doi: 10.55145/ajest . 2024.03.01.003.